



**HAL**  
open science

## Simulation tool for the Eddy current magnetic signature (EC-MS) non-destructive method

S. Zhang, B. Ducharne, Tetsuya Uchimoto, Aoba Kita, Y.A. Tene Deffo

### ► To cite this version:

S. Zhang, B. Ducharne, Tetsuya Uchimoto, Aoba Kita, Y.A. Tene Deffo. Simulation tool for the Eddy current magnetic signature (EC-MS) non-destructive method. *Journal of Magnetism and Magnetic Materials*, 2020, 513, pp.167221. 10.1016/j.jmmm.2020.167221 . hal-02971015

**HAL Id: hal-02971015**

**<https://hal.science/hal-02971015>**

Submitted on 22 Aug 2022

**HAL** is a multi-disciplinary open access archive for the deposit and dissemination of scientific research documents, whether they are published or not. The documents may come from teaching and research institutions in France or abroad, or from public or private research centers.

L'archive ouverte pluridisciplinaire **HAL**, est destinée au dépôt et à la diffusion de documents scientifiques de niveau recherche, publiés ou non, émanant des établissements d'enseignement et de recherche français ou étrangers, des laboratoires publics ou privés.



Distributed under a Creative Commons Attribution - NonCommercial 4.0 International License

# Simulation tool for the Eddy Current Magnetic Signature (EC-MS) non-destructive method.

S. Zhang<sup>1</sup>, B. Ducharne<sup>2,3</sup>, T. Uchimoto<sup>3,4</sup>, A. Kita<sup>1</sup>, **Y.A. Tene Deffo<sup>5</sup>**

<sup>1</sup>. Graduate school of Engineering, Tohoku University, Sendai, Japan.

<sup>2</sup>. LGEF, INSA Lyon, Villeurbanne, France.

<sup>3</sup>. Université de Lyon, Tohoku University, International Joint Uni, ELYTMAX UMI 3757, Sendai, Japan.

<sup>4</sup>. Tohoku University, Institute of fluid science IFS, Sendai, Japan.

<sup>5</sup>. **Faculty of Engineering and Technology, University of Buea, Buea, Cameroon.**

## **Abstract**

Magnetism has been used for years as a subsidiary method to identify the level of mechanical residual stress through ferromagnetic steels. It is admitted that residual stress strongly modifies the magnetic behavior and consequently the monitored magnetic signatures. However, some of them like the Eddy Current Magnetic Signature (EC-MS) happen to be especially sensitive. EC-MS exhibits drastic changes, strong enough to predict and anticipate the presence of elastic or plastic deformations. The EC-MS signature is obtained by plotting the imaginary part versus the real part of an Eddy current probe impedance, controlling locally a tested sample under the influence of a slowly varying high amplitude magnetic excitation. The superimposition of the weak amplitude, high-frequency magnetic excitation of the Eddy current probe to the quasi-static contribution creates minor hysteresis loop situations where the reversible magnetic contribution is the main provider. EC-MS is, therefore, an exceptional way to observe and characterize this reversible contribution and this over different average magnetic states. This contribution tends to be particularly sensitive to residual stresses and strains, and so is EC-MS. In this article, the Jiles-Atherton-Sablik theory and an improved Dodd and Deeds analytical solution for the simulation of a pancake-type Eddy current coil are combined to simulate EC-MS. From the simulation results, we illustrate and understand why EC-MS is so sensitive to residual stress. Eventually, we justify this method as probably the most indicated magnetic method for the control and evaluation of residual stresses through structural and construction steels.

## **Key words**

Eddy current magnetic signature, residual stress, Jiles-Atherton-Sablik theory, Dodd and Deeds analytical solution, hysteresis.

## Introduction

Magnetic non-destructive testing (NDT) consists in locally evaluating the integrity of ferromagnetic counterparts thanks to their magnetic signatures [1]. Under the influence of an external magnetic field, the magnetic answer of a tested sample will reflect its content, its nature and its history [2]-[4]. Since many years now, magnetic NDT has been used in steel production or by steel users companies to check the uniformity and the conformity of their products [5]. More recently it has also been used as a structural health monitoring tool in domains such as transportation or electrical energy production. Even if the magnetic Barkhausen noise (MBN) method is now commonly used in production lines of bearings and gear boxes, international standards allowing comparisons and reducing the influence of the human factor are still missing. The reason of this absence comes probably from the variety and the versatility of the magnetic sensors as well as the random nature of the tested samples geometry. We measure electrical quantities which are scalar images of the physical properties. As a consequence, to be efficient, micro-magnetic NDT needs calibration steps from well-known samples or time consuming adjustments where the settings rely on the time variation of the sensor signals. Magnetic NDT includes a large number of methods. Even if they have different names, most of them depend on similar physical behaviors, i.e. the interaction between the micro-structure and the local magnetization of the tested samples [6]. The increasing demand for quality improvement is of great motivation for researchers of this field. Two research objectives are particularly clear:

\_ To establish the most appropriate indicator for the evaluation of a targeted structural property (hardness, residual stress and strain, aging and fatigue ...) [7].

\_ To propose new methods/techniques by mixing simulations and experimental results and be able to return exact micro-structural properties [8].

In order to reach these two objectives, in the case of mechanical residual strains and stresses, recent works described in [9][10] by Matsumoto et al. with a method named Eddy Current Magnetic

Signature (EC-MS) and derived from the so called 3MA magnetic incremental permeability [11][12] seem particularly promising. Detailed in this article is a large dependence on the EC-MS signature to mechanical stresses in case of low carbon steel materials. Strong changes can be observed on the trajectory of the EC-MS signature of free to move samples, pre-stressed by different levels of unidirectional mechanical stress excitation as shown in Fig. 1 [10]:

\_ An anticlockwise circle-like shape (black loop at the right of Fig. 1), for a weak mechanical pre-stressed level, i.e. below the yield point.

\_ A single curve (blue loop at the right-hand of Fig. 1), for a pre-stressed strong enough to reach the Lüders-strain region.

\_ A clockwise circle-like shape for a pre-stressed treatment at the work hardening zone (red loop at the right of Fig. 1).

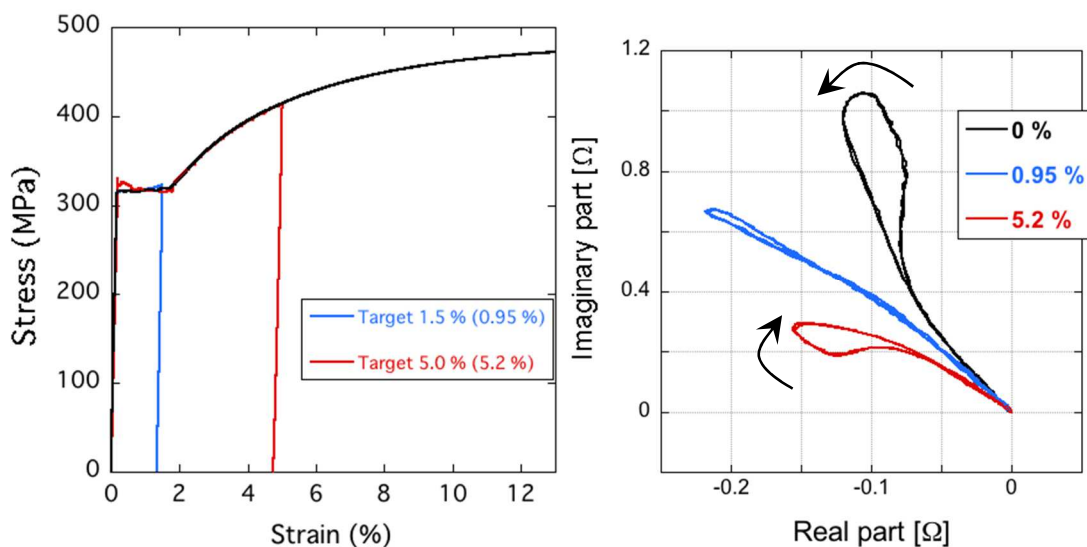


Fig. 1 – Experimental EC-MS signatures under different mechanical stress level [10].

By analyzing the EC-MS trajectory derived from low carbon steel materials, it is possible to establish the mechanical stress history of a tested specimen. EC-MS can be measured simultaneously to the magnetic incremental permeability (MIP) as both these magnetic signatures rely on the same

experimental situation [13][14]. While MIP focuses on the impedance magnitude of the Eddy current probe sensor, EC-MS consists of plotting its imaginary versus real part.

The resulting trajectory in the complex impedance plane is the characteristic signature of the EC-MS method. From a magnetic point of view, EC-MS just as MIP are strongly connected to the magnetic reversible contribution. This magnetisation contribution is classically observed in the Rayleigh zone of the first magnetisation curve, i.e. under weak external magnetic excitation, high enough to bend and distort the domain walls in a reversible way but low enough to unpin them from their hooking sites. MIP and EC-MS experimental situations barely reproduce the Rayleigh zone magnetic behaviour, the only difference is the average magnetic state of the tested sample which is incrementally changing due to the superimposed quasi-static magnetic excitation. MIP and EC-MS experimental observations show strong correlations to the mechanical state (stresses, strains ...), confirming indirectly the strong mechanical state dependence of the reversible magnetic contribution. In this article, a simulation scheme based on both the Jiles-Atherton-Sablik theory [15]-[17] and an improved Dodd and Deeds analytical solution [18][19] for the simulation of a pancake-type Eddy current coil are combined to simulate EC-MS. From the good correlation of our simulation results with the experimental ones:

\_ Underseek the strong influence of the reversible contribution in the EC-MS signature.

\_ Infer arguments telling why EC-MS is so sensitive to residual stress.

\_ Eventually, justify this method as probably the most indicated magnetic method for the control and evaluation of the residual stresses levels through structural and construction steels.

We recall the Jiles-Atherton-Sablik model in the first part of this article. An improvement is proposed to optimize the incremental permeability magnitude calculation. The second part is dedicated to the modified Dodd and Deeds analytical solution for the simulation of the experimental pan-cake type eddy current probe. The frequency dependence extension of the J-A-S model and the way we combined it to the D&D analytical solution come after. The experimental setup is detailed in the

fourth part and the last part is dedicated to comparisons simulations/experimental results and to some related comments. The general conclusion comes right after.

## Model

### Extended Jiles-Atherton-Sablik model

In 1984, D.C. Jiles and D.L. Atherton published their first of a long series of articles titled “theory of ferromagnetic hysteresis”, dedicated to the macroscopic simulation and understanding of the magnetic mechanisms ruling the ferromagnetic materials [20]-[22]. The richness of their theory relies on a limited number of parameters and on the strong commitment from both the authors to physically justify every equation of their simulation approach. The restrictions of their theory in its early stage are: the limitation to scalar situation (i.e. where the magnetic excitation  $H$  and state  $M$  are supposed to be collinear), the independence to the excitation frequency and the accommodation issue which is observed under minor loop situations and corresponds to the incapability of the model to simulate closed minor loops. According to the J-A theory, the total magnetic state  $M$  of a ferromagnetic material can be decomposed into its reversible ( $M_{rev}$ ) and irreversible ( $M_{irr}$ ) contributions [23].

$$M = M_{rev} + M_{irr} \quad (1)$$

In the model, the anhysteretic magnetization can be described by a Langevin-type equation [24]:

$$M_{anh} = M_s \left[ \coth\left(\frac{H_e}{a}\right) - \frac{a}{H_e} \right] \quad (2)$$

The anhysteretic magnetization can be considered as the magnetic state of a ferromagnetic material made out of magnetic domains moving through a defects and obstacles free mater. It can also be described by a hyperbolic sigmoid function:

$$M_{anh} = M_s \tanh\left(\frac{H_e}{a}\right) \quad (3)$$

$M_{anh}$  is the anhysteretic magnetization,  $M_s$  the saturation magnetization and  $a$  an anhysteretic magnetization trajectory parameter. According to the J-A theory,

$$a = \frac{k_b \theta}{\mu_0 m} \quad (4)$$

in which  $k_B$  is the Boltzmann's constant,  $\theta$  the temperature, and  $m$  the magnetic magnitude at a domain scale (most of the time equal to  $M_s$ ).

$H_e$  is the effective field, it is defined in eq. 5 below. It can be assimilated to the equivalent magnetic field observed locally by the ferromagnetic material. It includes the external magnetic excitation and a complementary contribution due to the surrounding magnetized area and modulated from  $\alpha$  a mean field parameter related to the inter domain coupling (see J-A theory [20]-[22])

$$H_e = H + \alpha M \quad (5)$$

The anhysteretic, the irreversible and reversible magnetizations are linked in Eq. (6):

$$M_{rev} = c(M_{an} - M_{irr}) \quad (6)$$

$c$  is a proportionality coefficient. It can be obtain experimentally by calculating the ratio between the initial differential susceptibilities of the first and the anhysteretic magnetization curves (Rayleigh zone) [22].  $c$  is especially influent for MIP and EC-MS simulations where the reversible magnetization is preponderant.

The anhysteretic and irreversible magnetization are connected through their derivatives and  $k$  the domain wall pinning parameter, as illustrated in Eq. 9:

$$\frac{dM_{irr}}{dH_e} = \frac{M_{anh} - M_{irr}}{k\delta} \quad (7)$$

$k$  is the pinning parameter, according to the J-A's theory it is linked to the average energy required to break pinning site in the magnetic material.  $\delta$  is just a directional parameter which ensures that energy is always lost through dissipation [20].

$$\begin{cases} \delta = +1 & \text{if } dH / dt \geq 0 \\ \delta = -1 & \text{if } dH / dt < 0 \end{cases} \quad (8)$$

Combining the equations above leads to the expression of the differential permeability:

$$\frac{dM}{dH} = \frac{(1-c) \frac{dM_{irr}}{dHe} + c \frac{dM_{anh}}{dHe}}{1 - \alpha(1-c) \frac{dM_{irr}}{dHe} - \alpha c \frac{dM_{anh}}{dHe}} \quad (9)$$

This differential permeability is obtained as a final step of the J-A time resolution algorithm. Its  $H$  integration leads to the induction field as illustrated below:

$$B(t) = \mu_0 \cdot \left( H(t) + \int \frac{dM}{dH} (t-dt) dH \right) \quad (10)$$

The incremental permeability can be evaluated in a simultaneous way by replacing in the time resolution algorithm eq. 5 with Eq. 11 (Fig. 2):

$$\begin{cases} \text{if } \text{sign}\left(\frac{dH(t)}{dt}\right) = \text{sign}\left(\frac{dH(t-dt)}{dt}\right) \\ H_{e_{MIP}}(t) = H(t-dt) - dH(t) + \alpha M(t-dt) \\ \text{else} \\ H_{e_{MIP}}(t) = H_e(t) \end{cases} \quad (11)$$

The magnetic incremental effective field  $H_{e_{MIP}}(t)$  is a virtual effective field simulating a sign change in the excitation field time derivation. Replacing  $H_e$  by  $H_{e_{MIP}}$  in the simulation process leads to a permeability expression (Eq. 9) which can be considered as the incremental permeability:

$$\frac{dM}{dH_{MIP}} = \frac{(1-c) \frac{dM_{irr}}{dHe_{MIP}} + c \frac{dM_{anh}}{dHe_{MIP}}}{1 - \alpha(1-c) \frac{dM_{irr}}{dHe_{MIP}} - \alpha c \frac{dM_{anh}}{dHe_{MIP}}} \quad (9)$$

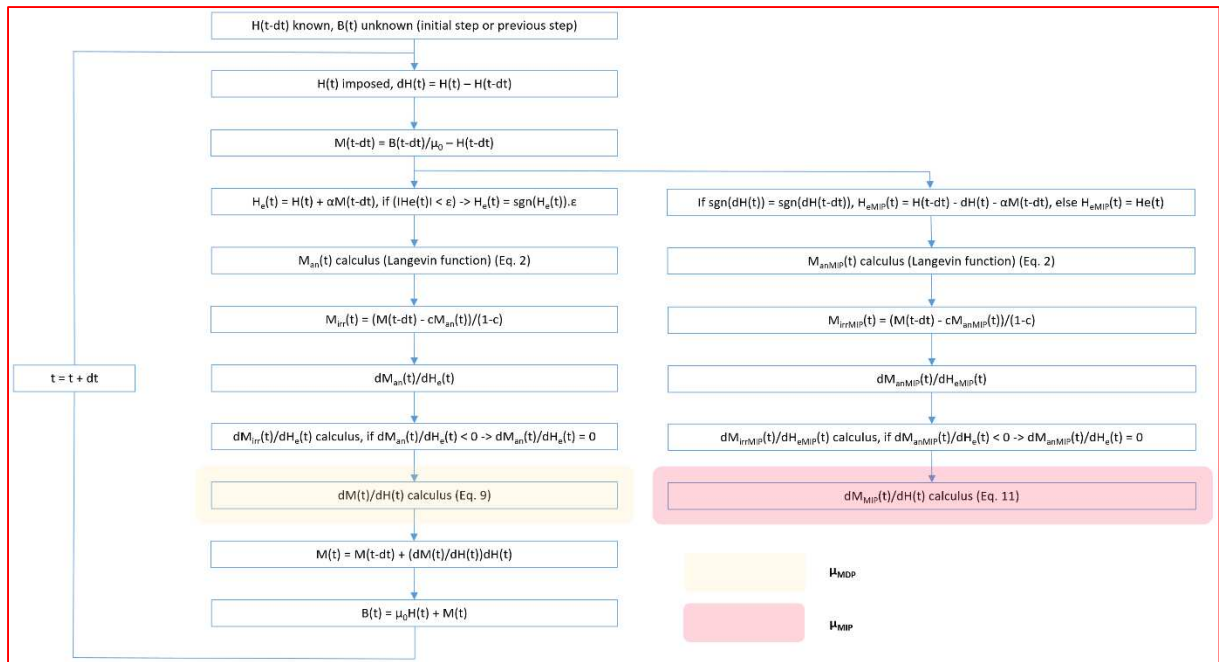
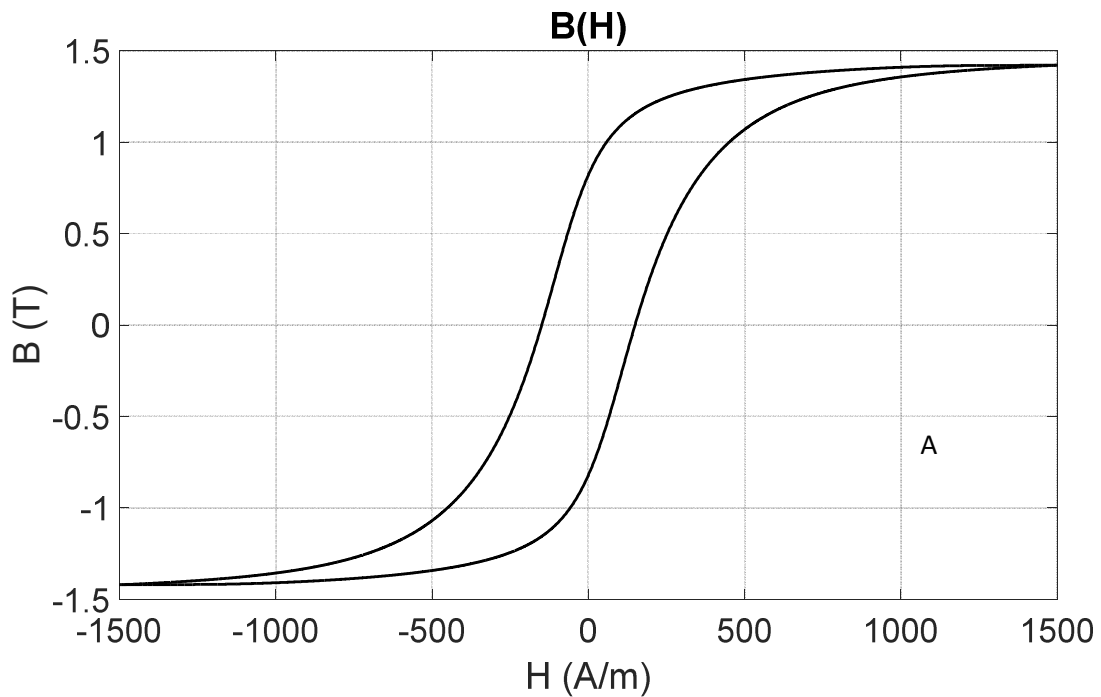


Fig. 2 – Time resolution algorithm of the J-A model and its extension to the calculus of the incremental permeability.

Fig. 3 gives an illustration of a simulated major  $B(H)$  hysteresis cycle and its related differential and incremental permeability.



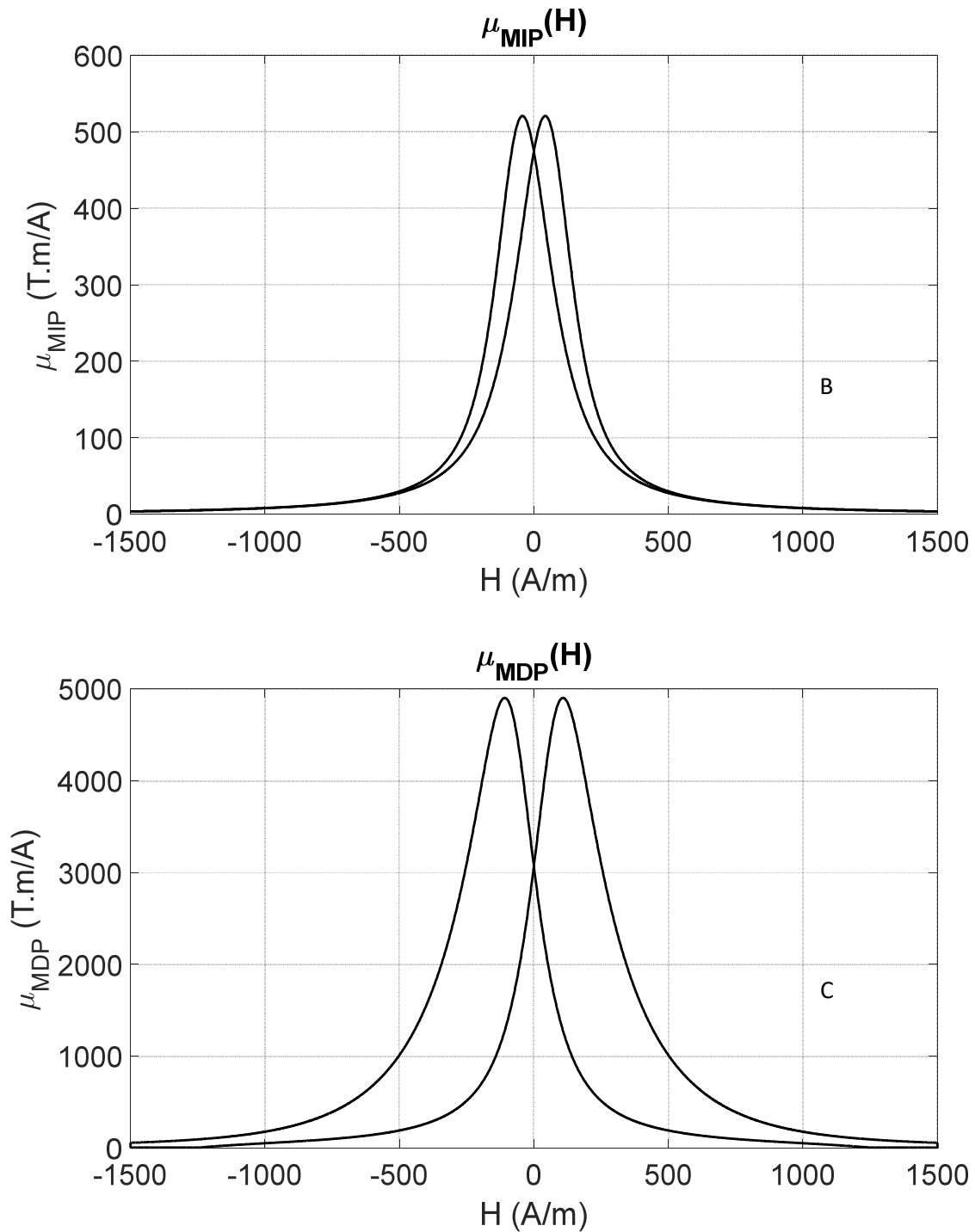


Fig. 3 – A  $B(H)$  hysteresis cycle, 3 – B Differential permeability  $\mu_{diff}(H)$ , 3 – C Incremental permeability  $\mu_{MIP}(H)$ .

Simulating the magnetic incremental permeability this way, is very convenient. It is fast and it avoids the real simulation of the minor loops. It indirectly solves the accommodation issue.

The extension of the J-A model proposed by Sablik and al. in [15]-[17] for the consideration of the magneto-mechanical effects goes on with the same philosophy, i.e. a lump simulation approach and

a limited number of parameters. Even if this model has limitations, it has been widely used because of its relative consistency with experimental results. It consists in considering the effect of stress on the magnetization state  $\lambda(M)$  as an additional perturbation of the effective magnetic field. Eq. 5 becomes:

$$H_e = H + \alpha M + H_T \quad (5)$$

Where  $H_T$  is the effective field contribution due to stress:

$$H_T = \frac{3}{2} \frac{T_0}{\mu_0} \left( \frac{\partial \lambda}{\partial M} \right)_T (\cos^2 \theta - \nu \sin^2 \theta) \quad (12)$$

$\theta$  is the angle between the applied stress  $T_0$  axis and the magnetic field  $H$  one.  $\nu$  is the Poisson's ratio.

Please note that in this study, we limit our investigation field to  $\theta = 0$ , i.e.  $H$  and  $T$  applied axis are similar, and Eq. 12 is reduced to:

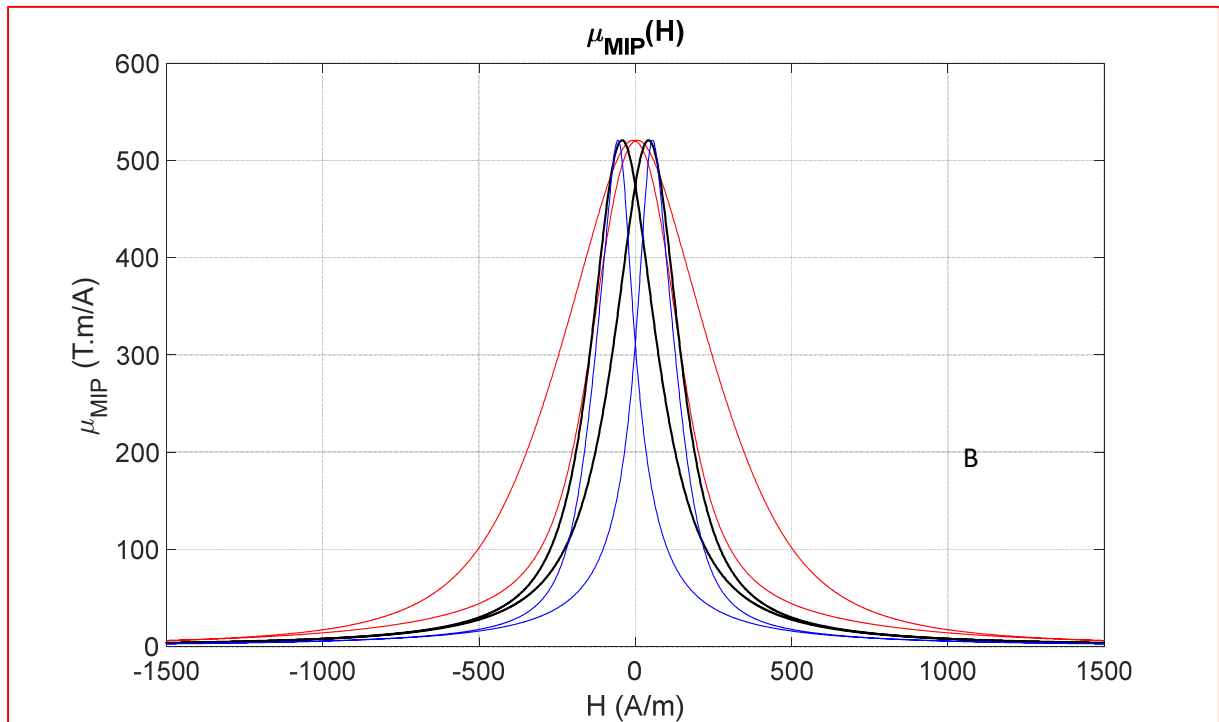
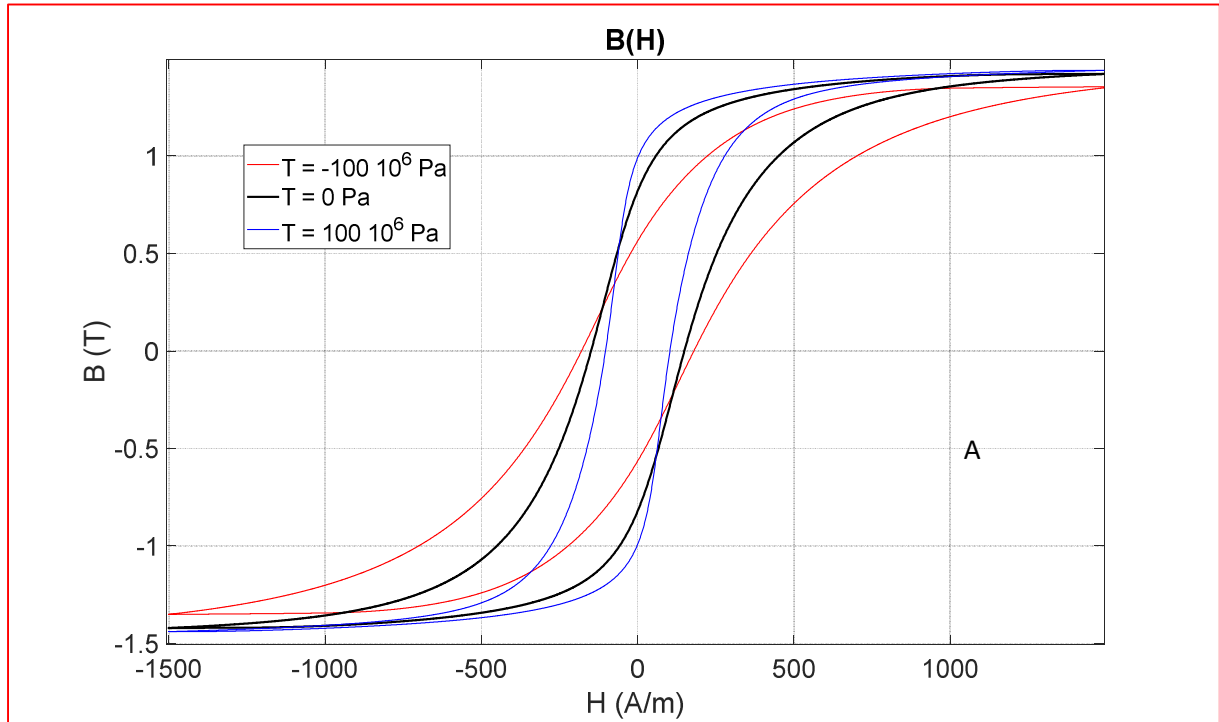
$$H_T = \frac{3}{2} \frac{T_0}{\mu_0} \left( \frac{\partial \lambda}{\partial M} \right)_T \quad (12)$$

The magnetostriction  $\lambda(M,T)$  is a Taylor series function, symmetric about  $M = 0$  (magnetization) and usually approximated by:

$$\lambda = \sum_{i=0}^{\infty} \gamma_i(T) \cdot M^{2i} \approx [\gamma_{11} + \gamma_{12}(T)] M^2 + [\gamma_{21} + \gamma_{22}(T)] M^4 \quad (13)$$

The parameter pairs  $(\gamma_{11}, \gamma_{22})$  and  $(\gamma_{12}, \gamma_{21})$  are respectively the stress independent and stress dependent components of the magnetostriction curve  $\lambda(M,T)$ , since the equivalent stress field operates through the magnetostriction. They are obtained from the truncated Taylor series function approximated to the quadratic and quartic parts. It should be noted that equation (13) stands as an approximation (developed from an empirical approach [25][26]) to the unknown domain configuration throughout the material; relating to the bulk magnetostriction and to the bulk magnetization under applied stress. Fig. 4 below illustrates the effect of an homogeneous uniaxial external stress on the evolution of the  $B(H)$  hysteresis cycle, and on both the differential and incremental permeabilities. The incremental permeability is calculated through the J-A-S extended version of Eq. 11:

$$\begin{cases} \text{if } \text{sign}\left(\frac{dH(t)}{dt}\right) = \text{sign}\left(\frac{dH(t-dt)}{dt}\right) \\ H_{e_{MIP}}(t) = H(t-dt) - dH(t) + \alpha M(t-dt) + H_T(t) \\ \text{else} \\ H_{e_{MIP}}(t) = H_e(t) + H_T(t) \end{cases} \quad (11)$$



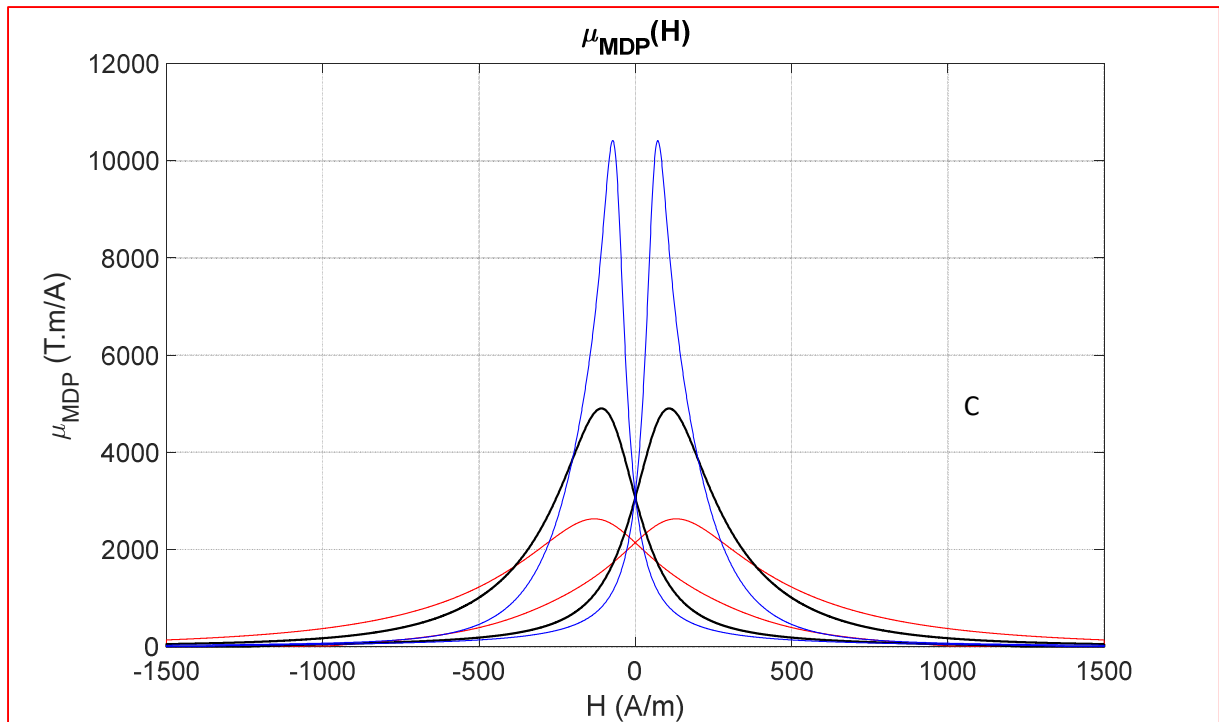


Fig. 4 – A B(H) hysteresis cycle, 4 – B Differential permeability  $\mu_{diff}(H)$ , 4 – C Incremental permeability  $\mu_{MIP}(H)$ .

The extension of the J-A-S is convenient for the simulation of the magnetic incremental permeability signature which is the evolution of the complex permeability magnitude as a function of the surface magnetic excitation field. From a quantitative point of view, the extended method is more than 10 times faster than the classic method. However there is no way to plot the EC-MS signature from this simulation method as we have no access to the B and H phase shift during the minor loops situations. To address this issue, in the next part of this article, we propose to use an improved frequency dependent Dodd and Deeds analytical solution for the impedance of the pan cake coil used in the experimental setup.

#### Extended Dodd and Deeds simulation

The Dodd and Deeds analytical solution for the simulation of an Eddy-current probe coil problem consists in an axisymmetric eddy current problem. The excitation is provided by a cylindrical coil, i.e. a circular coil with rectangular cross-section. The coil is located above a conductive half-space which can be layered or not. The coil is supposed to be supplied from a harmonic-type voltage and so is the current crossing through. In [10] Matsumoto and al. extended the classic D & D approach to

ferromagnetic materials. A frequency dependent losses term is added to take into account the microscopic eddy currents caused by the domain wall movements. These movements occur over the fixed potential energy due to the fixed static extern magnetic field excitation H, just like under the MIP and the EC-MS experimental situation. In this extended version and because of the additional term, the material permeability is no more constant and becomes frequency dependant:

$$\mu_e = \frac{\mu_{DC}}{1 + \rho(B)j\omega\mu_{DC}} \quad (14)$$

$\mu_e$  is the effective permeability and  $\mu_{DC}$  the quasi-static material permeability.  $\rho$  is a material magnetic dumping losses parameter. This parameter is supposed to be constant but correct simulation results of the EC-MS signature can only be obtained while giving  $\rho$  a B linear dependence [10].

$$\rho = \nu B + \rho_0 \quad (15)$$

Where  $\rho_0$  is the value of  $\rho$  under demagnetized state and  $\nu$  a constant depending on the nature of the ferromagnetic material.

#### Dynamic Jiles-Atherton-Sablik model

Both the J-A-S model and its inverse version J-A-S<sup>-1</sup> in their original configuration are limited to quasi-static situations, i.e. under a varying excitation field of limited dynamic (lower than the quasi-static frequency threshold). In [23] authors proposed a frequency dependent extension of the J-A<sup>-1</sup> model by the adjunction of a dynamic contribution, product of a constant  $\rho$  to the time derivation of the magnetic induction B. The resulting dynamic model equation is given below (Eq. 16):

$$\rho \frac{dB(t)}{dt} = H_{dyn}(t) - JA^{-1}(B(t)) \quad (16)$$

Here, J.A<sup>-1</sup> stands for the H(B) inverse quasi-static Jiles-Atherton hysteresis model [27]-[29]. Please note that from a dynamic simulation point of view both the J.A<sup>-1</sup> and the J.A.S<sup>-1</sup> models can be taken into account equally, therefore in Eq. 14 the J.A<sup>-1</sup> model can naturally be replaced by the J.A.S<sup>-1</sup> one (Eq. 17):

$$\rho \frac{dB(t)}{dt} = H_{dyn}(t) - JAS^{-1}(B(t)) \quad (17)$$

Where  $J.A.S^{-1}$  stands for the H(B) inverse quasi-static Jiles-Atherton-Sablik hysteresis model. The parallel between  $\rho$  the dynamic  $J-A^{-1}$  model constant and the D&D frequency dependent constant defined previously is evident. Both have the same physical meaning and should ideally exhibit the same value. To be consistent with this observation and converge towards a unique simulation base, in the dynamic  $J.A.S^{-1}$   $\rho$  can be replaced by  $\rho(B)$  as resumed in the system 18 below:

$$\begin{cases} \rho(B) \frac{dB(t)}{dt} = H_{dyn}(t) - JAS^{-1}(B(t)) \\ \rho(B) = \nu B + \rho_0 \end{cases} \quad (18)$$

Eventually, the final equation becomes:

$$(\nu B + \rho_0) \frac{dB(t)}{dt} = H_{dyn}(t) - JAS^{-1}(B(t)) \quad (19)$$

In the last part of this work, comparisons “simulations/measurements” for B(H) dynamic hysteresis cycles will be proposed to check if correct simulation results can be obtained using  $\nu$  and  $\rho_0$  the dynamic parameters set under EC-MS situation and to confirm the universality of these parameters.

### Coupled J-A-S / D&D simulation techniques for the EC-MS consideration

The J-A-S model has been described in the first part of this article. This simulation method gives access to the incremental permeability of a ferromagnetic material under a slowly varying high amplitude magnetic excitation and this for different levels of uniaxial mechanical stress. The J-A-S model in its scalar version as introduced here works under the assumption of the collinearity between B and H. Consequently, the incremental permeability simulated is supposed to be under  $\Delta H$  and  $\Delta B$  variations in agreement to this assumption. Unfortunately, the Eddy-current pancake-style probe coil used in the MIP and EC-MS experimental situation creates  $90^\circ$   $\Delta H$  excitation variations, as illustrated in Fig. 5 below. Both the AC and the DC excitation contributions are perpendicular vector quantities but the quasi-static excitation field maximum amplitude is typically from 100 to 1000 times higher than the AC one. Consequently in the scanned area the direction of the vector cumulative excitation field  $\vec{H}$  ( $\vec{H}_{DC} + \vec{H}_{AC}$  contribution) remains almost constant during a large

proportion of the quasi-static magnetization process. Based on the drastic difference between the AC and the DC excitation amplitude contributions such as the isotropic magnetic property of the material tested here, we will consider the incremental permeability simulated by the J-A-S model similar to the one resulting from the Eddy-current probe solicitation.

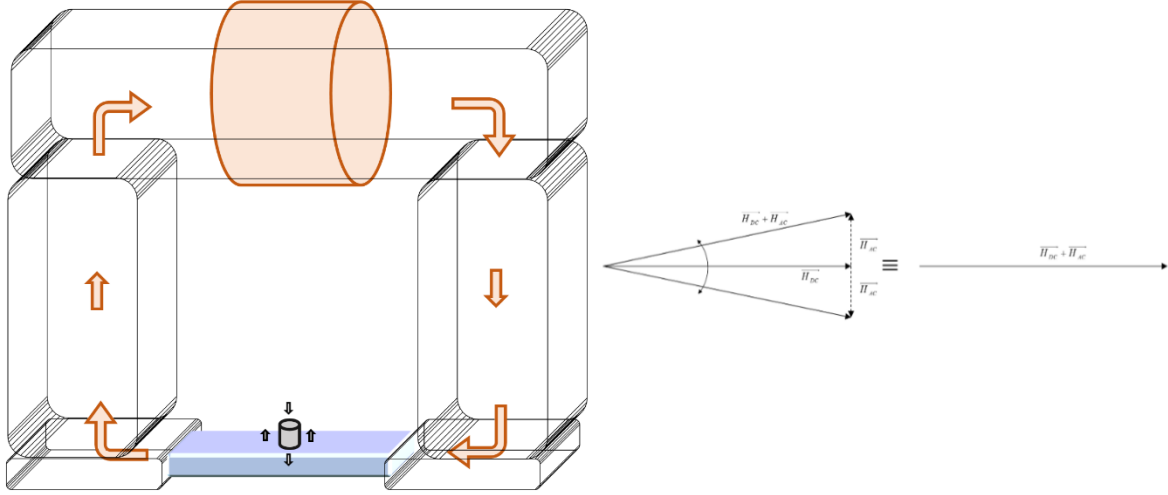


Fig. 5 – AC and DC magnetic contributions.

The first step of our simulation process consists in running the J-A-S model under a sinus magnetic excitation field and a constant level of mechanical stress. Once the J-A-S simulation done, the incremental permeability  $\mu_{MIP}^{J-A-S}(t)$ ,  $B(t)$  and  $\rho(B,t)$  are available for every step time of the simulation. In the second simulation step, the D&D simulation starts, setting  $\mu_{DC}^{D\&D} = \mu_{MIP}^{J-A-S}$  and  $\rho$  as a function of B (Eq. 20):

$$Z_{coil}^*(t) = Z_{coil}'(t) + iZ_{coil}''(t) = D \& D(\mu_{MIP}^{J-A-S}(t), \nu B(t) + \rho_0) \quad (20)$$

Where  $Z^*$ ,  $Z'$  and  $Z''$  are respectively the complex, the real part and the imaginary part of the sensor coil impedance,  $\mu_{MIP}^{J-A-S}$  is the incremental magnetic permeability calculated with the J-A-S model. At the end of the second step, both the real and the imaginary parts of the sensor coil impedance are available for every step time of the simulation. In the last steps of the simulation, both the first and the second steps are run again and this for all the different levels of mechanical stress required by the comparisons with the experimental results.

## Experimental situation

### Experimental setup

The overall 3D design of the effective experimental EC-MS setup is depicted in Fig. 6.

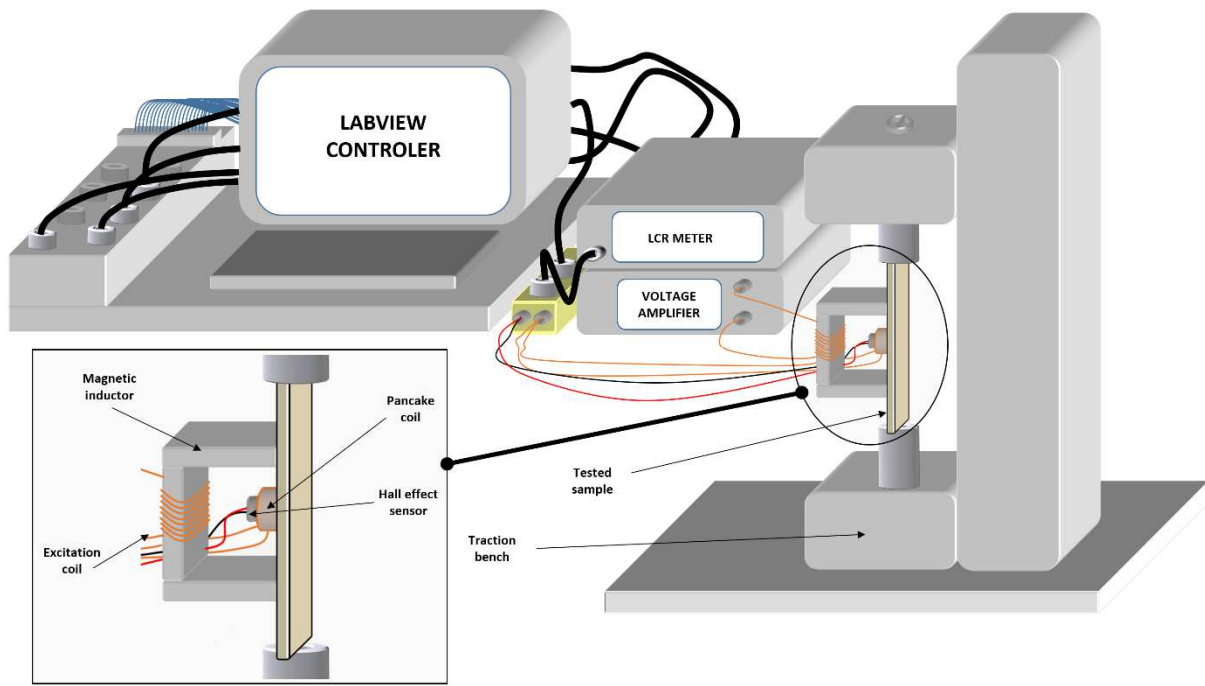


Fig. 6 – EC-MS experimental setup.

As illustrated in Fig. 6, for the EC-MS characterization, a quasi-static, 0.1 Hz sinusoidal alternating magnetic field  $H_{DC}$  is generated, it is driven up to the tested sample thanks to a U-shaped yoke magnetic circuit. The yoke is made out of iron silicon steel sheets. The yoke legs size is 10 mm × 20 mm and the inner-distance between legs is 20 mm. The amplitude is set to  $4 \cdot 10^5 \text{ A}\cdot\text{m}^{-1}$ . The tested sample is therefore slowly magnetized up to the saturation levels. A high frequency magnetic field  $H_{AC}$  is superimposed to this slowly changing magnetic state thanks to a pancake-type eddy current testing coil. The sensor information is: 3.3mm inner diameter, 3.95mm outer diameter, 3.0mm height, 275 turns, and 0.05mm wire thickness. These descriptive parameters will be used as input of the D&D simulation. During the whole process, the complex coil impedance is monitored using a LCR meter. Eventually, the local measurement of the tangent magnetic field strength  $H$  is measured by a hall sensor located in the middle of the pancake coil. Once the sensor complex voltage  $V$  is measured, its modulus can be plotted against the applied steady state magnetic field  $H_{DC}$  to obtain the classic

MIP butterfly loops. Its imaginary part  $V''$  can be plotted as a function of the real part  $V'$  to get the EC-MS signature. A constant mechanical traction strength is imposed using an INSTRON5582 universal testing machine at room temperature. The displacement is controlled using a clip gauge. The residual strain at the center of the specimen is measured using a 2 x 1.2 mm strain gauge. **The maximum tensile stress is limited to 170 MPa as the strain gauge is showing high risk of coming off for higher stress levels.**

Finally, this experimental setup can be used too, to measure the classic B(H) hysteresis cycles. The pancake-type eddy current testing coil is simply replaced by a surrounding one. The magnetic state B is estimated over integration of the new surrounding sensor coil electromotive force and the excitation magnetic field H measured with the Hall Effect sensor.

### Experimental specimens

The tested samples are 99.5 % pure iron ferromagnetic materials. The dimensions of the tensile test specimens are shown in Fig. 7 below. The thickness is 5 mm.

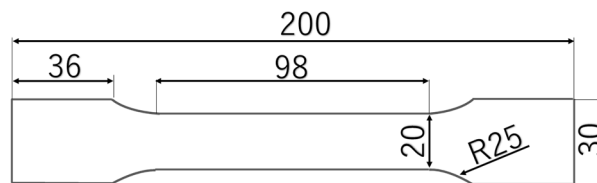


**Fig. 7 – Tensile test specimens dimensions.**

### Comparisons simulations/measurements

The first experimental situation simulated is the magnetic induction evolution of the pure iron sample under a 4 kA/m, 100 mHz (below the quasi-static threshold), sinus magnetic excitation H (Fig. 8). This simulation is necessary to set the J-A quasi-static parameters (Tab. 1, below). The best simulation results have been obtained using Eq. 21 sigmoid function as anhysteretic contribution:

$$M_{anh} = M_s \tan^{-1} \left( \frac{H_e}{a} \right) + bH_e \quad (21)$$

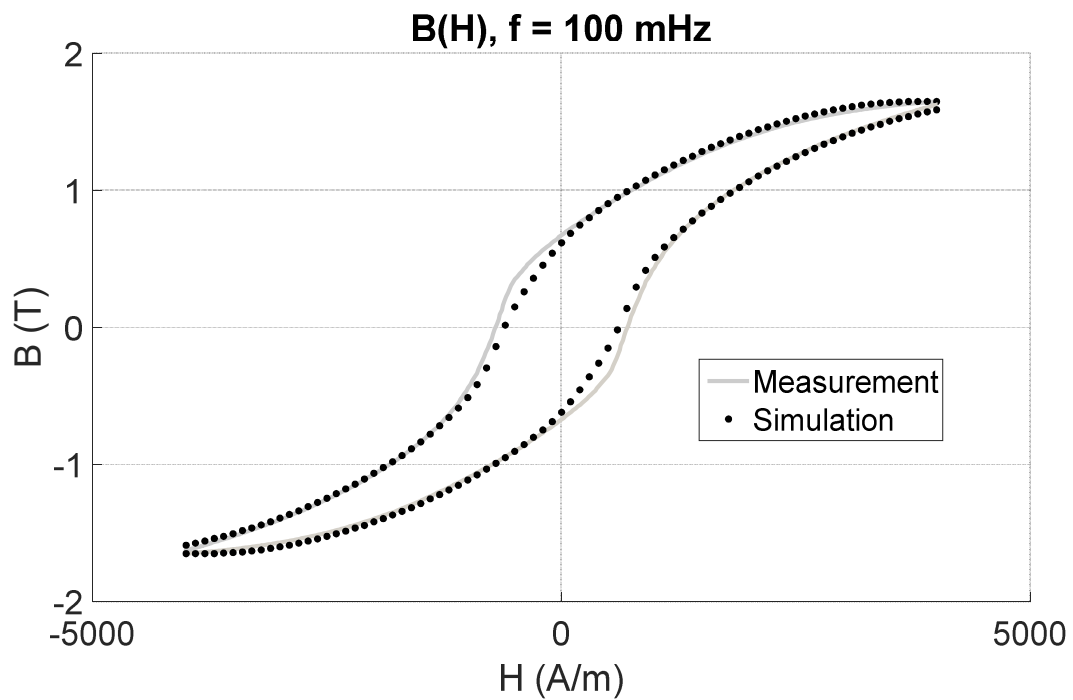


Fig. 8 – Comparison simulation/measure under quasi-static magnetic field excitation.

Tab. 1 – J-A quasi-static parameters.

| J-A Parameters | Typical value     |
|----------------|-------------------|
| b              | 99.4              |
| a              | 715               |
| Ms (A/m)       | $6.6 \cdot 10^5$  |
| k (A/m)        | 320               |
| c              | 0.5               |
| $\alpha$       | $3 \cdot 10^{-5}$ |

The experimental curve (Fig. 8) has been obtained using the experimental setup described in the “Experimental setup” subsection. As illustrated on Fig. 8, the good comparison obtained validates the simulation method.

The next experimental situations simulated are the MIP butterfly loops ( $I \nabla^* I(H)$ ) measured for different values of external mechanical stress. The stress levels have been set in order to test every domain of the stress vs strain curve (elastic deformations zone, Lüders band, plastic deformations zone). Just like in [10] and because of the unpredictable behavior of the sensor and of the acquisition setup (sensor wires, electrical contacts ...), the simulation needs a calibration step. A first comparison between the D&D simulation and an experimental result is performed using a well-known Inconel

paramagnetic steel ( $\theta = 1 \cdot 10^6 \text{ S.m}^{-1}$ ,  $\mu = \mu_0$ ) specimen. The Inconel is paramagnetic so the contribution of the local electrical eddy current field is relatively small. A rotation factor and an expansion factor were found so that the calculation result of the Inconel could be consistent with the experimental result in the impedance plane. A second test with the sensor coil “in the air” ( $\theta = 1 \cdot 10^{-10} \text{ S.m}^{-1}$ ,  $\mu = \mu_0$ ) far from any magnetic or conductive element is performed to validate the rotation factor and the expansion factor obtained with the first comparison. Tab. 2 below gives the correction factors corresponding to our experimental setup:

Tab. 2 – D & D correction factors.

| Correction factors   | Typical value |
|----------------------|---------------|
| Rotation factor (rd) | -1.46         |
| Expansion factor     | 1.348         |

Finally, the J-A-S model mechanical parameters have to be set, here again comparisons “simulation/measurement” are used. Tab. 3 gives these parameters:

Tab. 3 – J.A.S mechanical parameters.

| J-A-S Parameters | Typical value       |
|------------------|---------------------|
| $\gamma_{11}$    | $1 \cdot 10^{-19}$  |
| $\gamma_{12}$    | $-2 \cdot 10^{-29}$ |
| $\gamma_{21}$    | $2 \cdot 10^{-31}$  |
| $\gamma_{22}$    | $-2 \cdot 10^{-41}$ |

The anhysteretic simulation parameters depicted in Tab. 1 are obtained using the @Matlab curve fitting toolbox. The hysteresis and the mechanical parameters (Tab. 1 and 3) are set through an optimization method based on error functions (for more details, see [4][14]).

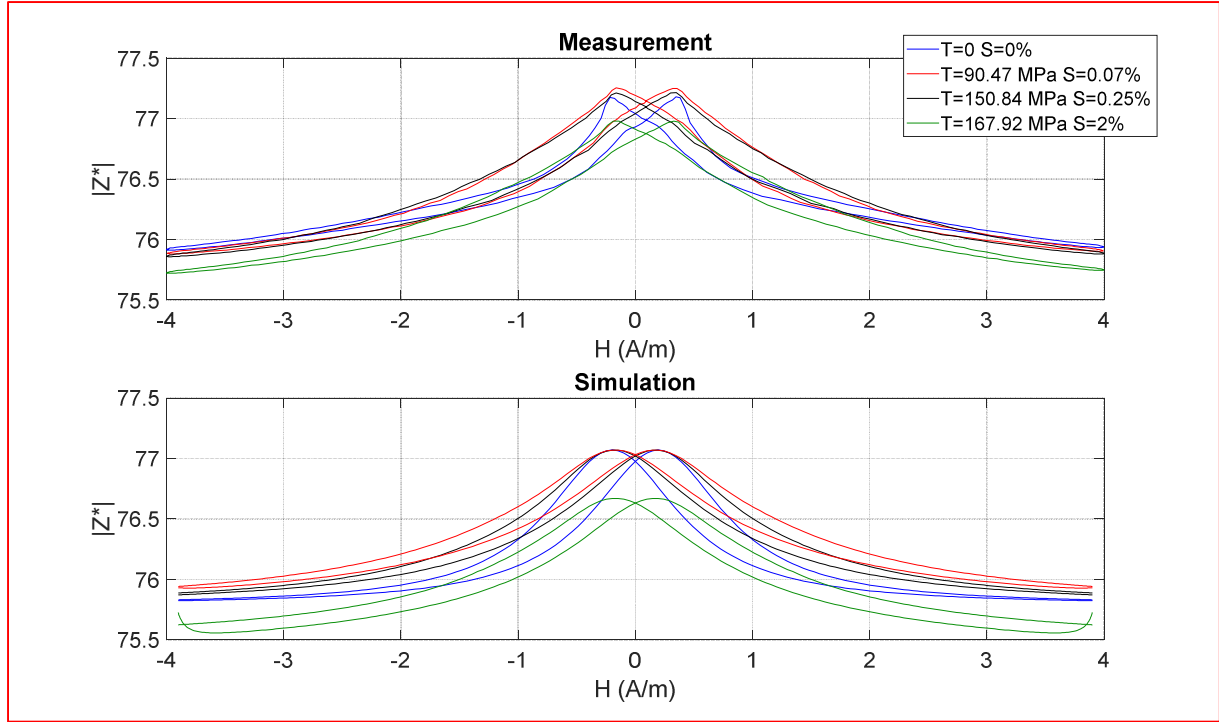


Fig. 9 – Comparisons simulation/measurement under MIP situations for different levels of external mechanical stress.

As illustrated on Fig. 9, the correct simulation tendencies obtained validate the combination “modified J-A-S model/ modified D&D” as a simulation tool of the  $IV^*I(H)$  MIP behavior (500 simulation steps were used per  $|Z^*|(H)$  butterfly loop).

The next simulation tests are dedicated to the EC-MS answers under the different mechanical stress levels. For these simulations, the dynamic simulation parameters,  $\nu$  and  $\rho_0$  have to be set. The comparison of the simulation and the EC-MS answers, under the absence of tensile stress gives dynamic parameters which can be conserved to anticipate the behavior under the influence of mechanical stress as proposed in the simulation part of this article. However, first simulations results show relatively poor accuracy and better results can be obtained by giving  $\nu$  and  $\rho_0$  a small T linear dependence, as described in Eq. 22 below:

$$\rho = \frac{1}{|T \cdot 10^{-7}|} (\nu B + \rho_0) \quad (22)$$

Tab. 4 gives the D&D dynamic parameters. Those parameters have been set under free to move mechanical conditions.

Tab. 4 – D&D dynamic parameters.

| J-A Parameters | Typical value |
|----------------|---------------|
| $\nu$          | 0.02          |
| $\rho_0$       | 0.006         |

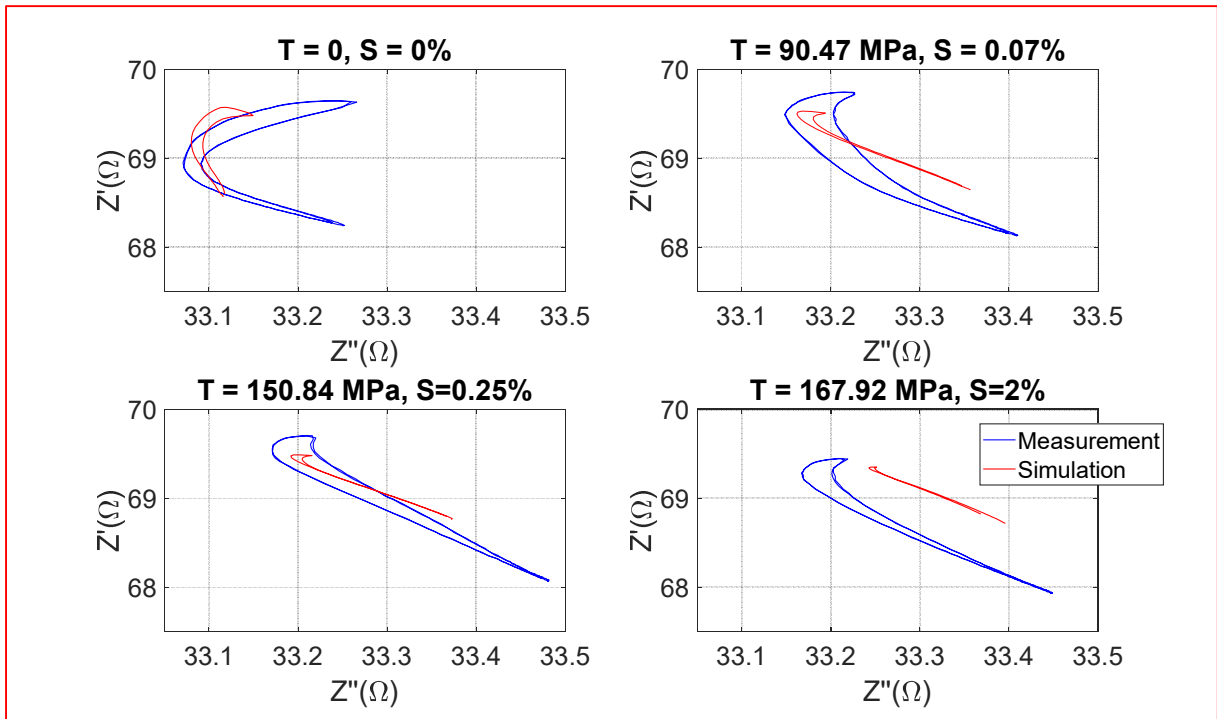
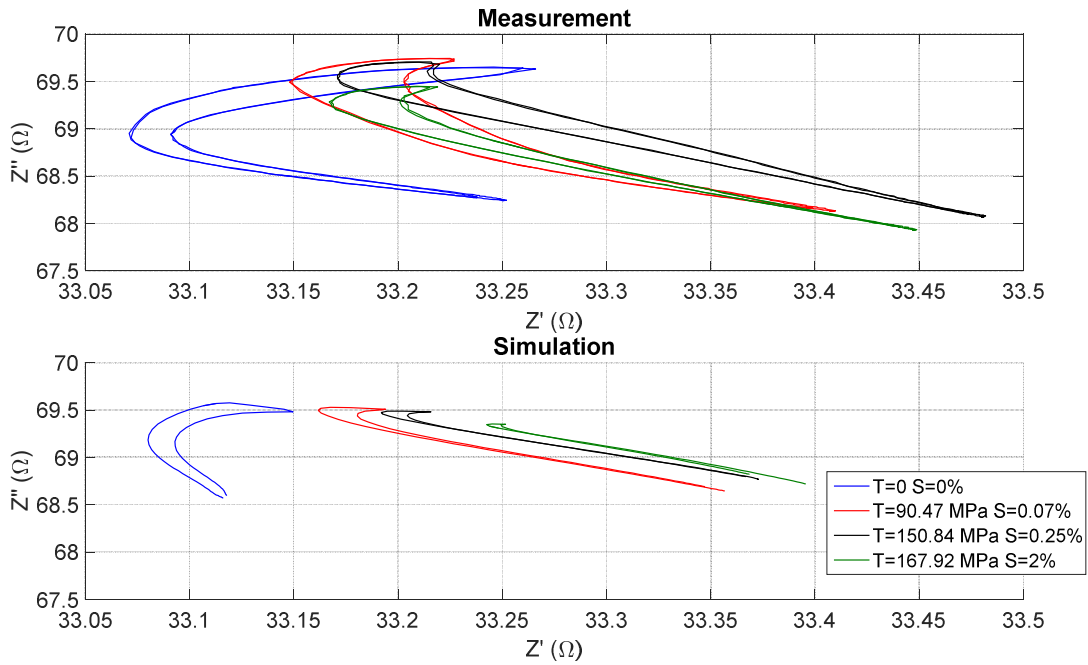


Fig. 10 – Comparisons simulation/measurement under EC-MS situations for different levels of external mechanical stress.

As illustrated on Fig. 10, here again the correct simulation results obtained validate the combination “modified J-A-S model/ modified D&D” as a simulation tool of the EC-MS behavior. It is worth noting, the small variations of the MIP coercivity Fig. 9 and the anticlockwise EC-MS trajectories Fig. 10. These observations lead to the conclusion of the limitation of all our experimental tests to the elastic deformation zone. The J-A-S in its original version is known to be more accurate in the elastic deformation zone, the good results observed in this study confirm this property.

Eventually, the last results consist in comparisons “simulations/measurements” for dynamic B(H) hysteresis cycles ( $f \in [0.5 \text{ Hz} - 80 \text{ Hz}]$ ). The objective of these last comparisons is to check if correct B(H) simulation results can be obtained using the dynamic parameter  $\rho(B,T)$  set for the simulation of the EC-MS experimental situation. In theory, both  $\rho$  the damping constant and  $\rho(B,T)$  the modified D&D dynamic parameter have the same physical meaning. Considering the relatively weak influence of the mechanical stress on  $\rho$ , for these tests, we neglect it and opt for an experimental situation where no tensile stress is imposed ( $T=0$ ) and the sample is free to move.

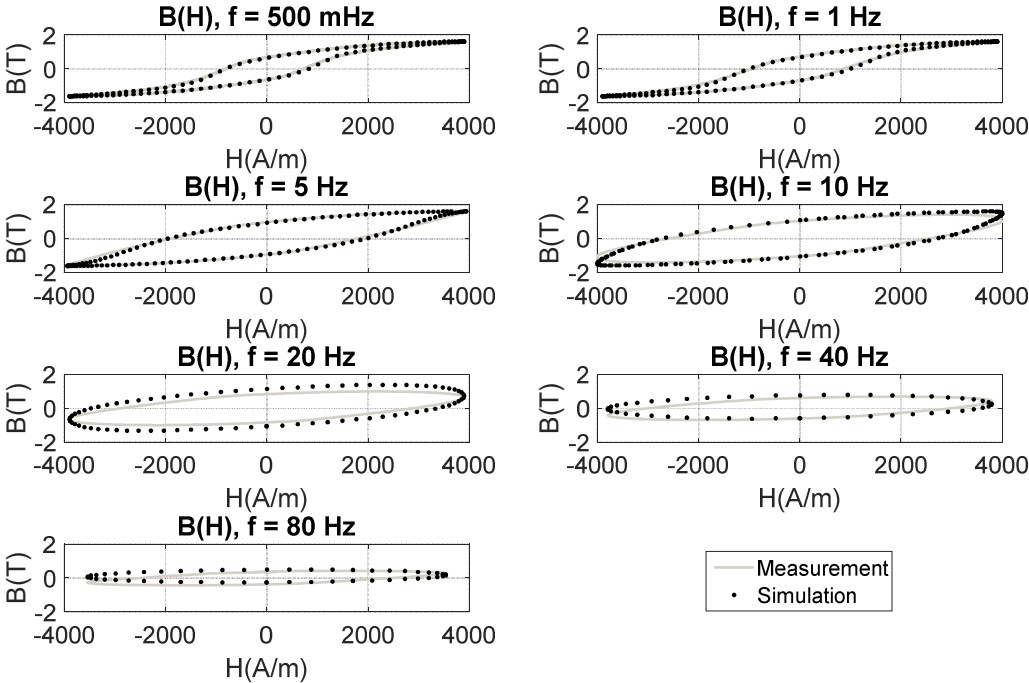


Fig. 11 – Comparisons simulations/measurements for the B(H) hysteresis cycles under different levels of excitation frequency.

As illustrated on Fig. 11, the B dependence of  $\rho$  has no consequence on the simulation accuracy. Even if the value of  $\rho$  is changing during the magnetization cycle, these variations are weak enough to create any observable consequence on the B(H) hysteresis cycle simulation for all the frequencies tested. From a physical point of view, these observations tend to say that the dynamic B (H) hysteresis cycle simulations are less sensitive to  $\rho$  variations than the EC-MS ones. The reversible magnetization is the preponderant contribution under EC-MS experimental situations... so is the irreversible magnetization for the hysteresis cycles. By combining these observations, we can deduce that  $\rho$  has a much stronger influence on the reversible magnetization than on the irreversible one.

## Conclusions

Eddy Current Magnetic Signature is probably the most mechanical stress sensitive magnetic indicator. This sensibility is obviously a very interesting property when it comes to non-destructive evaluation of mechanical residual stress. It is however a real challenge to simulate. Simulations of EC-MS are required as they constitute an essential step towards the understanding of the physical mechanisms. In this article, the scalar Jiles-Atherton-Sablik stress dependent hysteresis model has been used to simulate the induction, the differential and the incremental permeability of a mechanically stressed pure iron sample. By coupling these simulation results to a frequency dependent analytical solution of a pancake coil type Eddy current sensor (modified Dodds and Deeds analytical solution), the simulation of the EC-MS impedance variations have been obtained. To converge towards correct simulation results, the early stage D & D solution had to be improved by the adjunction of a classic dynamic contribution product of  $\rho$  to the time derivative of B. Unlike the classic approach, correct simulation results have only been obtained by considering a B and T small dependences of  $\rho$ , strong enough to modify the EC-MS signature (reversible magnetization) but too weak to influence the frequency dependence of the B(H) hysteresis cycles (irreversible magnetization).

Finally, the J-A-S model is supposed to give correct results on limited tensile stress levels. The good simulations obtained in this study are probably due to the relatively high yield point of the pure iron

samples tested. Even if the maximum of the mechanical stress were close to 170 MPa, all the magnetic signatures measured are typical from the elastic deformation zone. The perspectives of this research include comparison simulations/measurements under larger mechanical stress (beyond the yield point restriction) but the development of a new tensile stress sensing method is mandatory.

## References

- [1] Z.D. Wang, Y. Gu, Y.S. Wang, "A review of three magnetic NDT technologies", *J. of Mag. and Mag. Mat.*, vol. 324, Iss. 4, pp. 382-388, 2012.
- [2] D.C. Jiles, "Review of magnetic methods for nondestructive evaluation", *NDT Int.*, vol. 21, Iss. 5, pp. 311-319, 1988.
- [3] G. Dobmann, "Physical basics and industrial applications of 3MA-micromagnetic multiparameter microstructure and stress analysis", *Proc. ENDE Conf.*, pp. 1-12, 2007.
- [4] B. Gupta, B. Ducharne, T. Uchimoto, G. Sebald, T. Miyazaki, T. Takagi, "Non-destructive testing on creep degraded 12% Cr-Mo-W-V ferritic test samples using Barkhausen noise", *J. of Mag. And Mag. Mat.*, pp. 231-238, 2019.
- [5] M. Pelkner, V. Reimung, T. Kreutzbruck, "Size adapted GMR arrays for the automated inspection of surface breaking cracks in roller bearings", *Int. J. Appl. Electromag. Mech.*, vol. 45, pp. 473-479, 2014.
- [6] B. Gupta, T. Uchimoto, B. Ducharne, G. Sebald, T. Miyazaki, T. Takagi, "Magnetic incremental permeability non-destructive evaluation of 12 Cr-Mo-W-V Steel creep test samples with varied ageing levels and thermal treatments", *NDT & E Int.*, vol. 104, pp. 42-50, 2019.
- [7] J.W. Wilson, G. Y. Tian, S. Barrans, "Residual magnetic field sensing for stress measurement", *Sens. and Act. A: Physical*, vol. 135, Iss. 2, pp. 381-387, 2007.
- [8] Y. Li, J. Wilson, G. Y. Tian, "Experiment and simulation study of 3D magnetic field sensing for magnetic flux leakage defect characterization", *NDT&E Int.*, vol. 40, iss. 2, pp. 179-184, 2007.
- [9] T. Matsumoto, B. Ducharne, T. Uchimoto, "Numerical model of the Eddy Current Magnetic Signature (EC-MS) non-destructive micro-magnetic technique", *AIP Advance*, 035045, 2019.
- [10] T. Matsumoto, T. Uchimoto, T. Takagi, G. Dobmann, B. Ducharne, S. Oozono, H. Yuya, "Investigation of Electromagnetic Nondestructive Evaluation of Residual Strain in Low Carbon Steels Using the Eddy Current Magnetic Signature (EC-MS) Method", *J. of Mag. and Mag. Mat.*, vol. 479, pp. 212-221, 2019.
- [11] B. Wolter, Y. Gabi, C. Conrad, "Nondestructive testing with 3MA – An overview of principles and applications", *App. Sci.*, vol. 9, iss. 1068, 2019.
- [12] Y. Gabi, D. Böttger, B. Straß, B. Wolter, C. Conrad, F. Leinenbach, "local electromagnetic investigations on electrical steel FeSi 3% via 3MA micromagnetic NDT system", in *Proceedings of the 12th European Conference on Nondestructive Testing, ECNDT 2018, Gothenburg, Sweden, 11–15 June 2018*.
- [13] P. Meilland, P. Lombard, "Improved modelling of 3MA system's incremental permeability for on-line steel strip property assessment", *19<sup>th</sup> World Conference on Non-Destructive Testing (WCNDT)*, Munich, Germany, 2016.

- [14] B. Gupta, B. Ducharne, G. Sebald, T. Uchimoto, T. Miyazki, T. Takagi, "Physical interpretation of the microstructure for aged 12 Cr-Mo-V-W steel creep test samples based on simulation of magnetic incremental permeability", *J. of Mag. And Mag. Mat.*, vol. 486, 2019.
- [15] M.J. Sablik, D.C. Jiles, "Coupled magnetoelastic theory of magnetic and magnetostrictive hysteresis", *IEEE Trans. on Mag.*, vol. 29, iss. 4, pp. 2113, 1993.
- [16] J. Li, M. Xu, "Modified Jiles-Atherton-Sablik model for asymmetry in magnetomechanical effect under tensile and compressive stress", *J. Appl. Phys.*, vol. 110, n° 6, pp. 063918-1-063918-4, Sep. 2011.
- [17] M.J. Sablik, "A model for asymmetry in magnetic property behavior under tensile and compressive stress in steel", *IEEE Trans. on Mag.*, vol. 33, iss. 5, pp. 3958, 1997.
- [18] C.V. Dodd, W.E. Deeds, "Analytical solutions to eddy-current probe-coil problems, *J. Appl. Phys.*, vol. 39, pp. 2829-2838, 1968.
- [19] C.C. Cheng, C.V. Dodd, W.E. Deeds, General analysis of probe coils near stratified conductors, *Int. J. Non-destruct. Test.*, vol. 3, pp. 109-130, 1971.
- [20] D.C Jiles, D.L Atherton, "Theory of ferromagnetic hysteresis", *J. of Mag. and Mag. Mat.*, Vol. 61, pp. 48-60, 1986.
- [21] D.C. Jiles, D.L. Atherton, "Theory of ferromagnetic hysteresis". *J. App. Phys.* 55, pp. 2115, 1984.
- [22] D.C Jiles, D.L Atherton, "Ferromagnetic hysteresis", *IEEE Trans. on Mag.*, Vol. 19, pp. 2183-2185, 1983.
- [23] B. Zhang, B. Gupta, B. Ducharne, G. Sebald, T. Uchimoto, "Dynamic magnetic scalar hysteresis lump model, based on Jiles-Atherton quasi-static hysteresis model extended with dynamic fractional derivative contribution", *IEEE Trans. on Mag.*, iss. 99, pp. 1-5, 2018
- [24] R. Zwanzig, "Nonlinear generalized Langevin equations", *J. Stat. Phys.*, vol. 9, iss. 3, pp. 2215-2220, 1973.
- [25] D.C. Jiles, "Theory of the magnetomechanical effect", *J. Phys. D: App. Phys.*, vol. 28, pp. 1535-1546, 1995.
- [26] Y.A. Tene Deffo, P. Tsafack, B. Ducharne, B. Gupta, A. Chazotte-Leconte, L. Morel, "Local measurement of peening-induced residual stresses on iron nickel material using needle probes techniques", *IEEE Trans. on Mag.*, vol. 55, iss. 7, 2019.
- [27] J. V. Leite, N. Sadowski, P. Kuo-Peng, N. J. Batistela, J. P. A. Bastos, "The inverse Jiles-Atherton model parameters identification", *IEEE Trans. on Mag.*, vol. 39, n° 3, pp. 1397-1400, 2003.
- [28] J. V. Leite, N. Sadowski, P. Kuo-Peng, N. J. Batistela, J. P. A. Bastos, A. A. de Espinola, "Inverse Jiles–Atherton vector hysteresis model", *IEEE Trans. on Mag.*, vol. 40, n° 4, pp. 1769-1775, 2004.
- [29] Y. Bai, B. Ducharne, H. Jantunen, J. Juuti, "Simulation and validation of temperature-dependent ferroelectric properties of multifunctional BCZT and KBNNO ceramics", *Mat. Res. Exp.*, vol. 5, 116305, 2018.